Lab Report 1

Abstract

Dynamic windows with adjustable tints offer tremendous benefits in reducing energy use in the buildings; however, conventional dynamic window technologies are limited by their inability to achieve color neutrality and by their inability to be actively controlled by the users. To address these challenges, this study aimed to develop a new dynamic window that was close to being color neutral and can be actively adjusted by the users. In this study, platinum-modified (Pt-modified) fluorine tin oxide (FTO) working electrodes were prepared and reversible electrodeposition of Copper-Bismuth (Cu-Bi) had been employed on the Pt-modified FTO working electrodes. We hypothesized that the dynamic windows we fabricated in this study were able to maintain constant transmission values at both the clear state and the dark state regardless of the number of cycling. In this study, We used real real-time optical transmission measurements, cyclic voltammetry (CV), and four-point probe measurements to characterize the dynamic windows we fabricated. Specifically, our functional dynamic window with 5.5 cycles exhibited reversible cycling between the clear state with an average transmittance of 55% and the dark state with an average transmittance of 5%. Our functional dynamic window with 10 cycles exhibited reversible cycling between the clear state with an average transmittance of 30% and the dark state with an average transmittance of 10%. The functional dynamic window had the ability to be stably switched for at least 5 cycles when a voltage range of -1.00 V to 1.00 V was applied. Additionally, we estimated a maximum window edge size of 12.67 cm based on the measured average sheet resistance of 7.47 Ω from Lab 5 and the CV scan results from Lab 2.

Introduction

As human civilization progresses at an unprecedentedly fast pace, more energy is needed to keep the indoor environment comfortable for its inhabitants while giving its inhabitants access to natural light and views of the outdoors. The dynamic window technology with its ability to control the energy flow and reduce the energy cost is a perfect candidate to help solve this challenge. Dynamic windows with adjustable tints enable the users to dynamically and electronically control the flow of light and heat into and out of the building, therefore, offering tremendous benefits in reducing energy use in the buildings. As a result, dynamic windows have gained a lot of interest over the past several decades and many have explored various dynamic

window technologies including devices that use passive changes of tinting like the photochromic and thermochromic methods as well as devices that use active changes of tining like the electrochromic and chemochromic methods.

The devices that use passive changes of tinting or devices that use non-electrochromic materials, however, cannot be actively controlled by the users. Compared to passive tinting technologies, the electrochromic dynamic windows leverage the high light attenuation and reflection characteristics of the photochromics devices and utilize voltage to actively control metal deposition within the window. The materials that are used in the electrochromic dynamic windows have the property of changing colors or darkness as induced by electrostatic potentials or electrochemical reactions. Common electrochromic materials used in dynamic windows include liquid crystal, tungsten oxide (WO_3), and viologens. And the liquid crystal changes color upon an electric potential, whereas tungsten oxide and viologens change color in response to the electrochemical reactions.

However, there are still several challenges that remain in the dynamic window technologies despite recent advances in electrochromic materials. First, many of the current dynamic windows are not color neutral which makes the window absorptive for certain ranges of wavelengths of light, leading to poor heat management. Moreover, many of the materials like indium tin oxide (ITO) and viologens that are used in the current dynamic window technologies are expensive thus making dynamic windows difficult to scale.

In this study, we set out to fabricate two 25 cm^2 dynamic windows based on the reversible electrodeposition of Cu-Bi that can switch uniformly between clear and dark states. The devices consisted of a fluorine tin oxide (FTO) working electrode modified with Pt nanoparticles. The devices were filled with liquid electrolytes (5 mM $BiCl_3$, 15 mM $CuCl_2$, 60 mM HCl, and 1 M LiBr) that were used to perform the electrodeposition of Cu-Bi. After the fabrication was completed, we performed spectroscopic characterizations of the clear state and dark state of the dynamic windows. We also performed the strip-chart measurements of the windows using a 5-cycle trial and a 20-cycle trial. Finally, we applied four-point probe measurements to the windows to obtain the sheet resistance of the dynamic windows which enabled us to estimate the largest possible size of the dynamic window we can make while maintaining uniform deposition over the entire window area.

We hypothesized that the dynamic windows we fabricated were able to maintain a constant transmission value at the clear state and a constant transmission value at the dark state regardless of the number of cycling.

Experimental Design

Lab 1

Preparation of the Electrolyte

A 100-mL solution that contains 5 mM $BiCl_3$ and 15 mM $CuCl_2$ was made by dissolving 0.1577 grams of $BiCl_3$ and 0.2017 grams of $CuCl_2$ in the deionized (DI) water. To completely dissolve the precipitate, we first set up five 20 mL vials and then transferred 10 mL of the stock solution of $BiCl_3$ and $CuCl_2$ to each 20 mL vial. We then added various amounts of H^+ and Br^- to the solution by using HCl and LiBr.

We made, in total, five solutions with different amounts of H^+ and Br^- to optimize the concentrations of HCl and LiBr in the final solution that had all the precipitates dissolved. The information about these five solutions is shown in the table (Table1) below.

Table 1: The HCl concentration, the amount of HCl to add, the LiBr concentration, the amount of LiBr to weight, and the existence of precipitates of the five solutions we prepared in Lab 1.

HCl Concentration	How much HCl to add	LiBr Concentration	How much LiBr to weight	All Precipitates dissolved?
60 mM	50 µL	576 mM	0.5 g	Yes
60 mM	50 µL	288 mM	0.25 g	Yes
60 mM	50 µL	58 mM	0.05 g	Yes
100 mM	500 µL	35 mM	0.05 g	Yes
300 mM	250 µL	0 mM	0 g	No

Preparation of the Working Electrode

An indium tin oxide (ITO) slide, pretreated in a piranha solution (30 wt.% H_2O_2 : H_2SO_4 = 1:3 v/v), was used as the working electrode of the dynamic window. To make the ITO surface homogenous and to facilitate uniform nucleation of Cu and Bi particles across the area of the

ITO, we modified the ITO surface with Pt nanoparticles. We diluted 0.5 mL of the Pt nanoparticle stock dispersion to 10 mL in a petri dish with deionized (DI) water. The as-received 1cm by 2cm ITO slide with conducting layer that had a thickness of 180 nm was soaked in the prepared Pt nanoparticle solution for 60 minutes followed by rinsing with DI water and transferring onto a hot plate with a temperature set to 250 °C for 60 minutes. Then the ITO slide was stored in a dry petri dish.

Lab 2

Preparation of the Electrochemical Cell

To prepare the electrochemical cell, we first rinsed the cuvette with DI water. After the rinsing, we selected the electrolyte of interest and added it to the cuvette. The electrolyte was added to the cuvette until it is about $\frac{3}{4}$ full in order to not cover part of the alligator clip that was used to make electrical contact with the working electrode. A total of five electrolytes of interest were selected. In each trial of the experiment, one of the five electrolytes was selected and added to the cuvette. The information on the five electrolytes of interest is presented in Table 2 as shown below.

Table 2: The five electrolytes of interest that were used in the later cyclic voltammetry measurement. The electrolytes were numbered from one to five and each have different contents.

Electrolyte Numbering	Contents of the Electrolyte
Electrolyte 1	5 mM $BiCl_3$, 15 mM $CuCl_2$, 60 mM HCl, and 1 M LiBr
Electrolyte 2	5 mM $BiCl_3$, 60 mM HCl, and 1 M LiBr
Electrolyte 3	15 mM $CuCl_2$, 60 mM HCl, and 1 M LiBr
Electrolyte 4	60 mM HCl and 1 M LiBr
Electrolyte 5	5 mM $BiCl_3$, 15 mM $CuCl_2$, 60 mM HCl, and 288 mM LiBr

The potential, controlled by the electrochemical workstation, governs the voltage applied across the working and reference electrodes. We selected the modified ITO as the working electrode and placed it inside the electrolyte that was already in the cuvette. An alligator clip was

used to make electrical contact with the working electrode and the other end of the alligator clip was routed through the pre-drilled hole in the cuvette cap to connect to the potentiostat (Model SP-150, Bio-Logic Science Instruments). We then placed the reference electrode in the electrolyte through another hole in the cuvette cap. The reference electrode contains a silver wire coated with Ag/AgCl, which is soaked in a 3M NaCl solution and separated from the electrolyte by an ion-permeable membrane. Finally, the Pt counter electrode was placed in the electrolyte. An alligator clip was used to make electrical contact with the counter electrode in a manner similar to the one of the working electrode. Additionally, we checked our electrodes in the cuvette to make sure they did not touch one another at any point in our experiment.

Cyclic Voltammetry (CV)

The initial CV scan voltage (E_i) was the open-circuit voltage (E_{OC}). We then set the scan rate to be 50 mV/s. The range of scan was between -1.00 V and +1.00 V.

The cyclic cycles were then measured on each of the five solutions by sweeping the potential of the working electrode from -1.00 V to +1.00 V. The data for each of the five solutions were saved for further analysis.

Lab 3

Dynamic Window Fabrication

We assembled the window as shown in Figure 1. The conducting side of the FTO faced toward the edge seal rubber and the non-conducting side faced outward as shown in figure 1. Another FTO slide was used as the back glass by orienting its non-conducting side facing the edge seal rubber as shown in Figure 1.

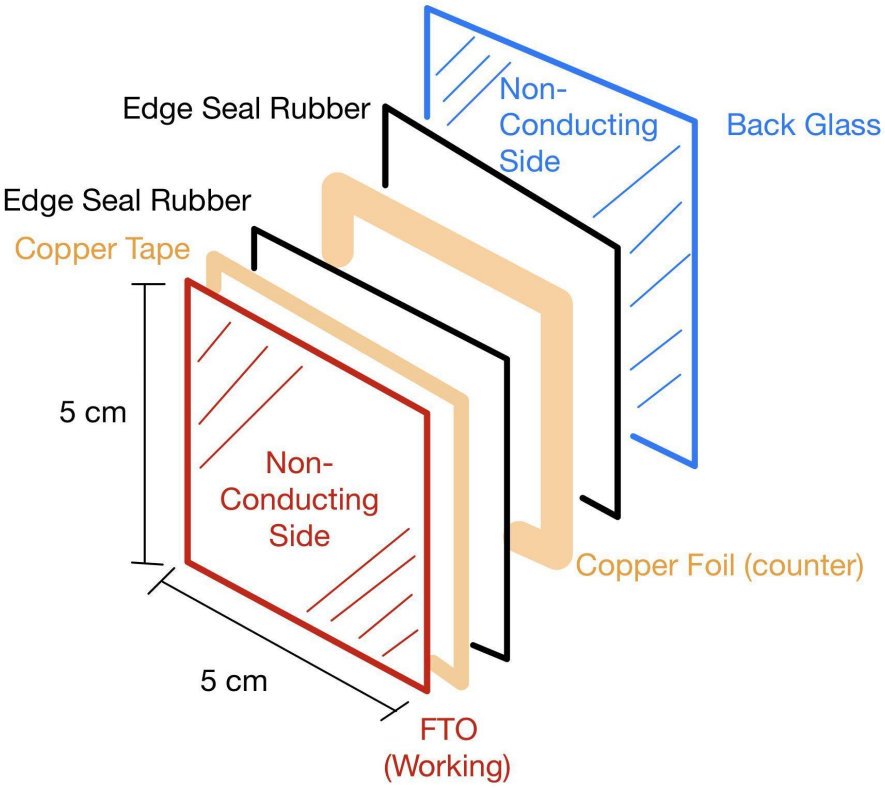

Figure 1: The schematic figure of different layers of the dynamic window with the correct orientation of each layer. The conducting side of the FTO (colored in red) faced toward the edge seal rubber and the non-conducting side faced outward. Another FTO slide (colored in blue) was used as the back glass by orienting its non-conducting side facing the edge seal rubber. The FTO colored in red served as the working electrode and would be connected to the negative end of the power source. The copper foil (colored in orange) served as the counter electrode and would be connected to the positive end of the power source.

We assembled the window with the following steps in order: assembly of the counter-electrode half of the dynamic window, assembly of the working-electrode half of the dynamic window, integration of both sides of the dynamic window, and injection of electrolyte and sealing of the window with epoxy.

To assemble the counter-electrode half of the dynamic window, we placed the edge seal rubber on the four edges on the non-conducting side of a pre-cleaned FTO slide. Then we cut the copper foil in the shape of the frame with a tab sticking out and place it on the edge seal rubber that was on the non-conducting side of a pre-cleaned FTO slide.

To assemble the working-electrode half of the dynamic window, we placed the copper tape over the four edges of the conducting side of a pre-cleaned FTO slide. We made one piece of the copper tape slightly longer than the rest for connection with an alligator clip. Then we placed the edge seal rubber on the four sides of the copper tape and the width of the edge seal rubber was larger than that of the copper tape.

To integrate both sides of the dynamic window, we turned over the FTO with copper tape with edge seal rubber and placed it over the counter-electrode half we had already assembled early on. To prevent potential shorts between the working and counter electrodes, we placed the tab of the copper foil and the tab of the copper tape away from each other. After the two sides of the window were assembled, we placed the window on the hot plate with a temperature set to 120 °C for 5 minutes.

After removing the window from the hot plate and having the window cool down to room temperature, we used 5-minute epoxy to seal most of the sides of the window, leaving a small portion uncovered for electrolyte injection, and let the epoxy cure for at least 15 minutes until it is no longer sticky. Then we placed the window on a stand with the epoxy-free corner pointing up and inserted a 25-gauge needle through the edge-seal rubber in the epoxy-free region as the vent. We used another 25-gauge needle to load the electrolyte without the hydroxyethyl cellulose (HEC) (2 wt. %) and injected the electrolyte through the epoxy-free edge-seal rubber. After the injection was completed, we removed both needles, made sure there was no leakage of electrolyte from the window, and sealed the epoxy-free corner with epoxy.

At the end of the dynamic window fabrication session, a total of two identical dynamic windows are made and their information is presented in Table 3 as shown below. However, one of the windows was broken and did not function when the cyclic voltammetry (CV) was applied to it. As a result, we applied a 5.5-cycle CV and a 10-cycle CV to the functional window when working on the dynamic window testing in lab 4.

Table 3: Fabrication information of the dynamic windows and the testing conditions of the windows. The fabrication information involves the types of transparent conductive oxide (TCO) electrode the windows used, the electrolyte the windows used, and the operating temperature of the windows. The testing conditions of the window involve the number of cyclic voltammetry (CV) cycles that would be applied to the windows.

Window Number (Condition)	Transparent Conductive Oxide (TCO) Electrode	Electrolyte	Operating Temperature	Number of Cycles
Window 1 (functional)	Fluorine Tin Oxide (FTO)	Liquid (5 mM $BiCl_3$, 15 mM $CuCl_2$, 60 mM HCl, and 1 M LiBr)	Room Temperature	5.5 cycles
Window 1 (functional)	FTO	Liquid (5 mM $BiCl_3$, 15 mM $CuCl_2$, 60 mM HCl, and 1 M LiBr)	Room Temperature	10 cycles
Window 2 (broken)	FTO	Liquid (5 mM $BiCl_3$, 15 mM $CuCl_2$, 60 mM HCl, and 1 M LiBr)	N/A	N/A

Lab 4

Spectroscopic Characterizations of the Dynamic Window

The setup of lab 4 experiment involved the following instruments: model SP-150 potentiostat from Bio-Logic Science Instruments, halogen light source HL-2000-FHSA from Ocean Optics, and model USB650 optical spectrometer from Ocean Optics.

We tested the two dynamic windows we made in lab 3 one at a time. For each window, we placed the dynamic window between the optical fiber for the light source and the fiber for light detection in the optical spectrometer setup. Then we turned on the halogen light source HL-2000-FHSA and checked if the light path was roughly perpendicular to the window. We then connected the tab of the copper tape to the alligator lead of the working electrode of the potentiostat, and the tab of the copper foil to that of the counter electrode.

To perform the spectroscopic characterizations of each of the dynamic windows, we took two spectra in the range 350 nm to 1000 nm, one with the window at the clear state (no voltage applied) and the other at the dark state (after applying -1V potential to the working electrode).

Strip-Chart Measurements of the Windows

To perform the strip-chart measurements of the window that is functional, we chose the 500 nm wavelength for sampling and set the range of CV scan between -1.00V and 1.00V at the scan rate of 50 mV/s. We held the potential at -1.00 V and 1.00 V each for 30 seconds. We

performed two trials for the strip-chart measurements of the functional window: one trial with 5.5 cycles and the other with 10 cycles. For each trial, we started the strip-chart measurement first, then start the CV scan. After the cycles were completed, we ended the CV scan before stopping the optical strip-chart measurement. Finally, we checked the saved files for both CV and optical strip charts to make sure they both have system time saved as the time stamp.

Lab 5

Four-Point Probe Measurements of TCO Substrates

We used the four-point probe model from Ossila to perform the four-point probe measurements of the TCO substrates. The setup of the four-point probe measurements is shown in figure 2 below.

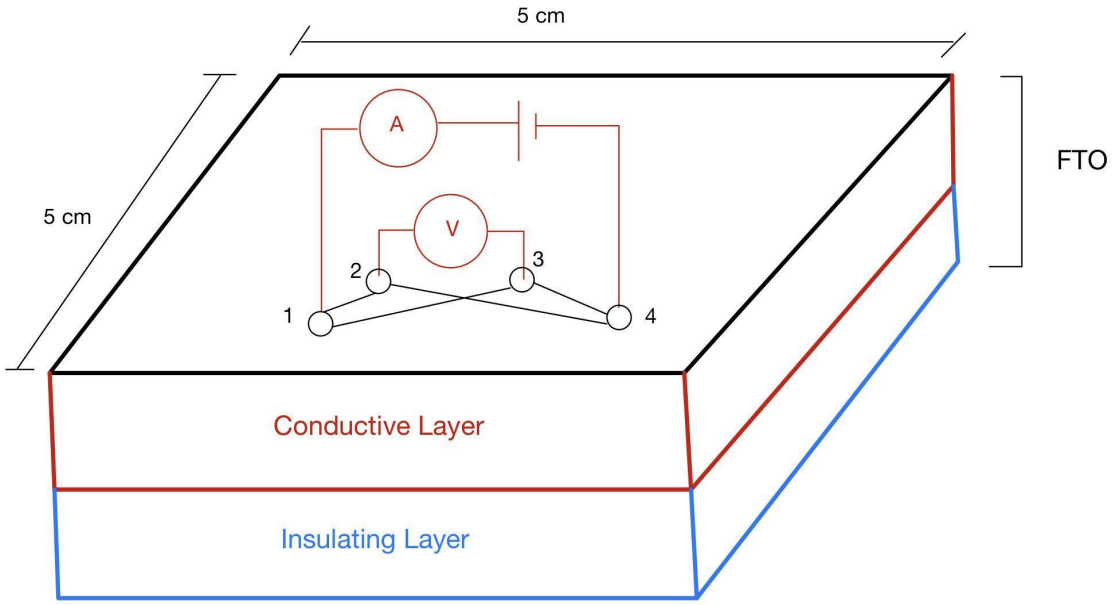

Figure 2: The setup of the four-point probe measurement of the TCO. The TCO we measured was a 5 cm by 5 cm FTO. All the probes were contacted with the conductive layer of the FTO.

All the probes contacted the conductive side of the TCO. The independent variable of the measurements was the current that passed through probe 1 and probe 4 and the dependent variable was the voltage between probe 2 and probe 3. We applied a current of 2mA through probe 1 and probe 4 and measured the voltage across probe 2 and probe 3. The type of TCO substrate we used was a 5 cm by 5 cm FTO. We performed the four-point probe measurements

under two different conditions using the same 5 cm by 5 cm FTO each with 100 repeats. For the first condition, we performed the four-point probe measurement on the dry FTO. For the second condition, we performed the four-point probe measurement with liquid electrolyte (5 mM $BiCl_3$, 15 mM $CuCl_2$, 60 mM HCl, and 1 M LiBr).

Results and Discussion

Lab 2

CV Graphs and Peak Assignments

For solution 1, based on Panel a and Panel b from Figure 3 as shown below, we assigned the peak at 0.25 V with 6.58 mA to the half-reactions of $Bi \rightarrow Bi^{3+}$ & $Cu \rightarrow Cu^{+}$. We assigned the peak at 0.56 V with 2.52 mA to the half-reaction of $Cu^{+} \rightarrow Cu^{2+}$. We assigned the peak at 0.01 V with -1.53 mA to the half-reaction of $Cu^{2+} \rightarrow Cu^{+}$. We assigned the peak at -0.36 V with -3.55 mA to the half-reaction of $Bi^{3+} \rightarrow Bi$. We assigned the peak at -0.53 V with -4.44 mA to the half-reaction of $Cu^{+} \rightarrow Cu$. Finally, we assigned the peak at-1.00 V with -4.66 mA to the half-reaction of $2H^{+} \rightarrow H_2$ (gas).

Based on Panel b from Figure 3 as shown below, we compared the differences between the curves for solutions 1 and 5. First, the peak of solution 5 for the $Bi \rightarrow Bi^{3+}$ half-reaction was lower than that of the $Bi \rightarrow Bi^{3+}$ & $Cu \rightarrow Cu^{+}$ half-reaction in solution 1. This was because the $Cu \rightarrow Cu^{+}$ half-reaction did not happen at the same time as the $Bi \rightarrow Bi^{3+}$ half-reaction in solution 5.

Second, the peak of the $Cu \rightarrow Cu^{2+}$ half-reaction in solution 5 shifted more to the right than those of the $Bi \rightarrow Bi^{3+}$ & $Cu \rightarrow Cu^{+}$ and $Cu^{+} \rightarrow Cu^{2+}$ half-reactions in solution 1. This difference was likely contributed by the fact it was more thermally difficult to transfer two electrons than just transferring one electron in a reaction. As a result, a higher voltage was required to overcome the thermal difficulty to carry out an entire $Cu \rightarrow Cu^{2+}$ reaction than the separate $Cu \rightarrow Cu^{+}$ and $Cu^{+} \rightarrow Cu^{2+}$ reactions. And this reasoning was also applicable to explain why we observed the peak of the $Bi^{3+} \rightarrow Bi$ & $Cu^{2+} \rightarrow Cu$ half-reactions in solution 5 shifted more to the left than those of $Bi^{3+} \rightarrow Bi$, $Cu^{2+} \rightarrow Cu^{+}$, and $Cu^{+} \rightarrow Cu$ half-reactions in

solution 1. Additionally, we observed that the peak of the Cu → Cu^{2+} half-reaction in solution 5 was higher than that of the Cu^{+} → Cu^{2+} half-reaction but lower than that of the Bi → Bi^{3+} & Cu → Cu^{+} in solution 1. We also observed that the peak of the Bi^{3+} → Bi & Cu^{2+} → Cu half-reactions in solution 5 had the same height as that of the Bi^{3+} → Bi half-reaction and was higher than that of the Cu^{+} → Cu half-reaction but was lower than that of the Cu^{+}→ Cu^{2+} half-reaction in solution 1.

Finally, we saw that the $2H^{+}$ → H_2 (gas) half-reaction in solution 5 was higher than that of the $2H^{+}$ → H_2 (gas) half-reaction in solution 1. This was likely due to the increase in overpotential of the experiment on solution 5 experiment caused by the deposition of Cu and Bi on the electrode from the experiments done on solutions 1, 2, and 3.

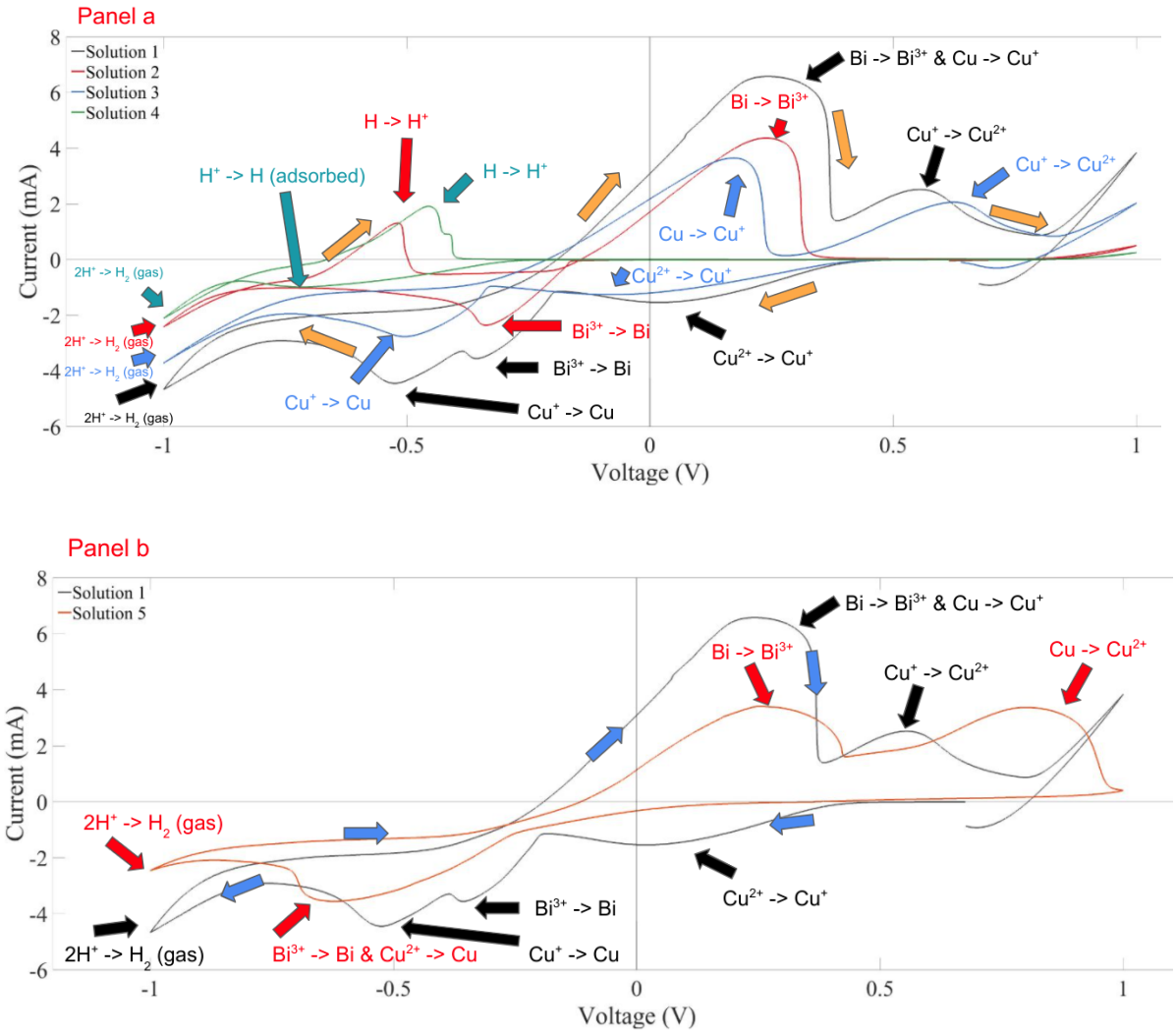

Figure 3: CV Scan of five different solutions. We used an Ag/AgCl reference electrode during all of our CV scans. Figure 3 Panel a represents the CV scan done on solutions 1 to 4 that used electrolytes 1 to 4 correspondingly from Table 2. Figure 3 Panel b represents the CV scan done on 1 and 5 that used electrolytes 1 and 5 correspondingly from Table 2.

Throughout all of our CV scans, as shown in Figure 3 above, we had chlorides in all the electrolytes. If chlorides were replaced with sulfates, then there would be no Cl^- ions in the electrolyte. It was noteworthy that the intermediate oxidation state of Cu(I) was stabilized by the Cl^- ions in the electrolyte. As a result, one should not expect to see two peaks corresponding to $Cu \rightarrow Cu^+$ and $Cu^+ \rightarrow Cu^{2+}$, but only one peak of $Cu \rightarrow Cu^{2+}$ due to the instability of Cu^+ in the aqueous solution without the Cl^- ions.

Lab 4

Spectroscopic Characterizations of the Windows (spectra and strip charts)

The results for this section were obtained from the experiments performed on window 1 with two testing conditions as shown in Table 3 from above. No experiments were performed on window 2 (as shown in Table 3 from above) since window 2 was broken. Based on Figure 4 Panel a and Panel c as shown below, we observed a deviation of transmission from 100% in the UV, visible, and near-infrared (NIR) regions in the clear state of the windows. This deviation was likely caused by the potential light absorbers in the dynamic window we fabricated. First, the glass of the dynamic window, which was located in the back glass and the working electrode, was a strong absorber below 400 nm which contributes to the non-UV transparency. Second, the dynamic window contained Cu^{2+} ions which absorb the red region (600-750 nm) of the visible spectrum. And finally, the FTO of our dynamic window was able to absorb NIR light above 750 nm.

Based on Figure 4 Panel b and Panel d as shown below, we observed that the dynamic window, regardless of the number of cycles, had lower transmission values in the dark state compared to the clear state. When the dynamic window was in the dark state, the deposition of metal within the window enabled the window to have more free electrons. And based on Drude model, the reflection of the window would increase and thus lead to a decrease in transmission.

Panel a

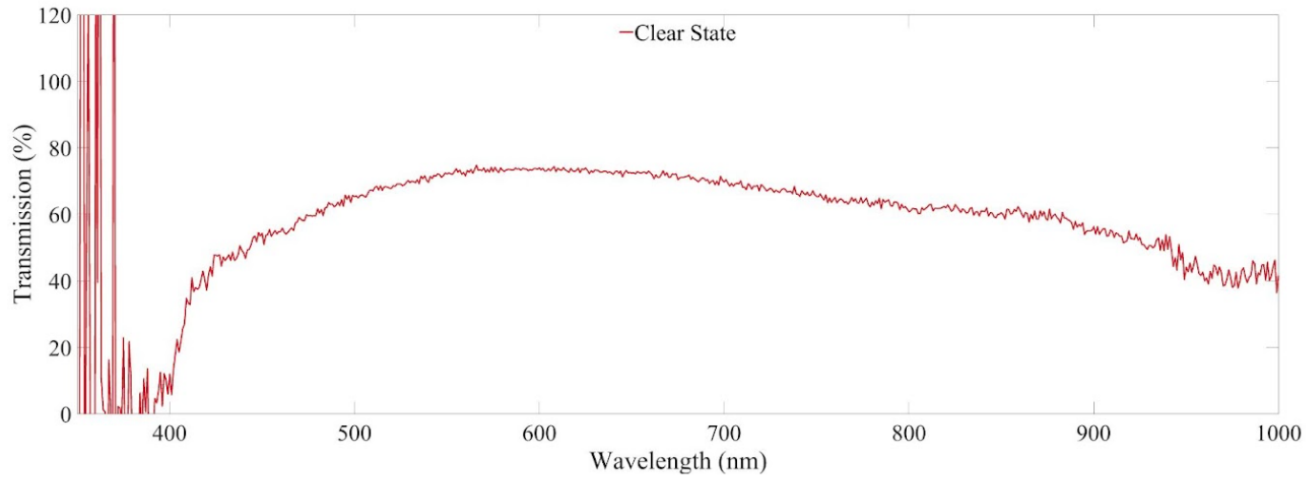

Panel b

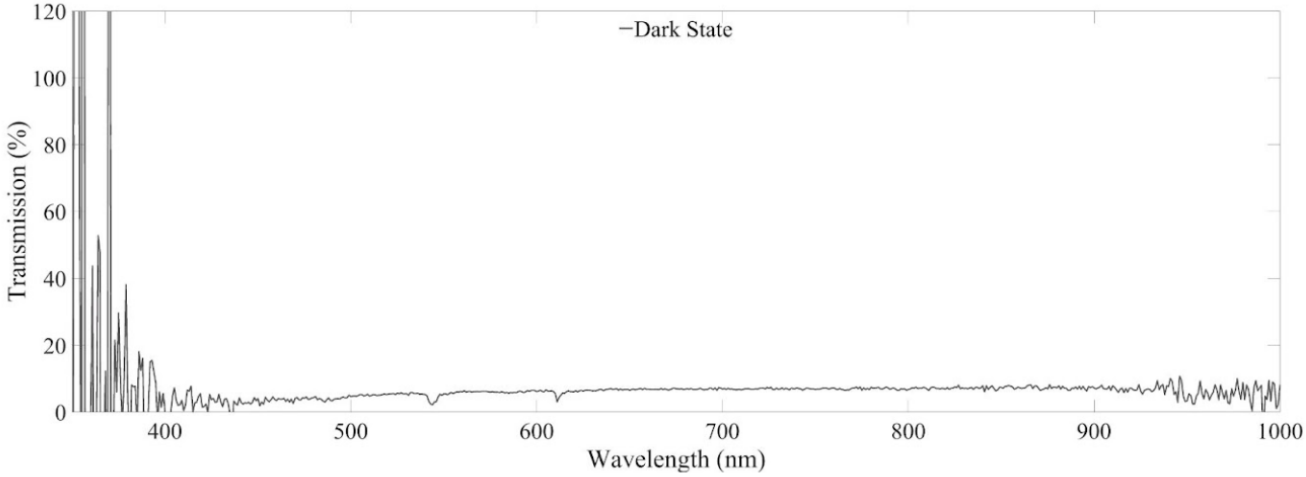

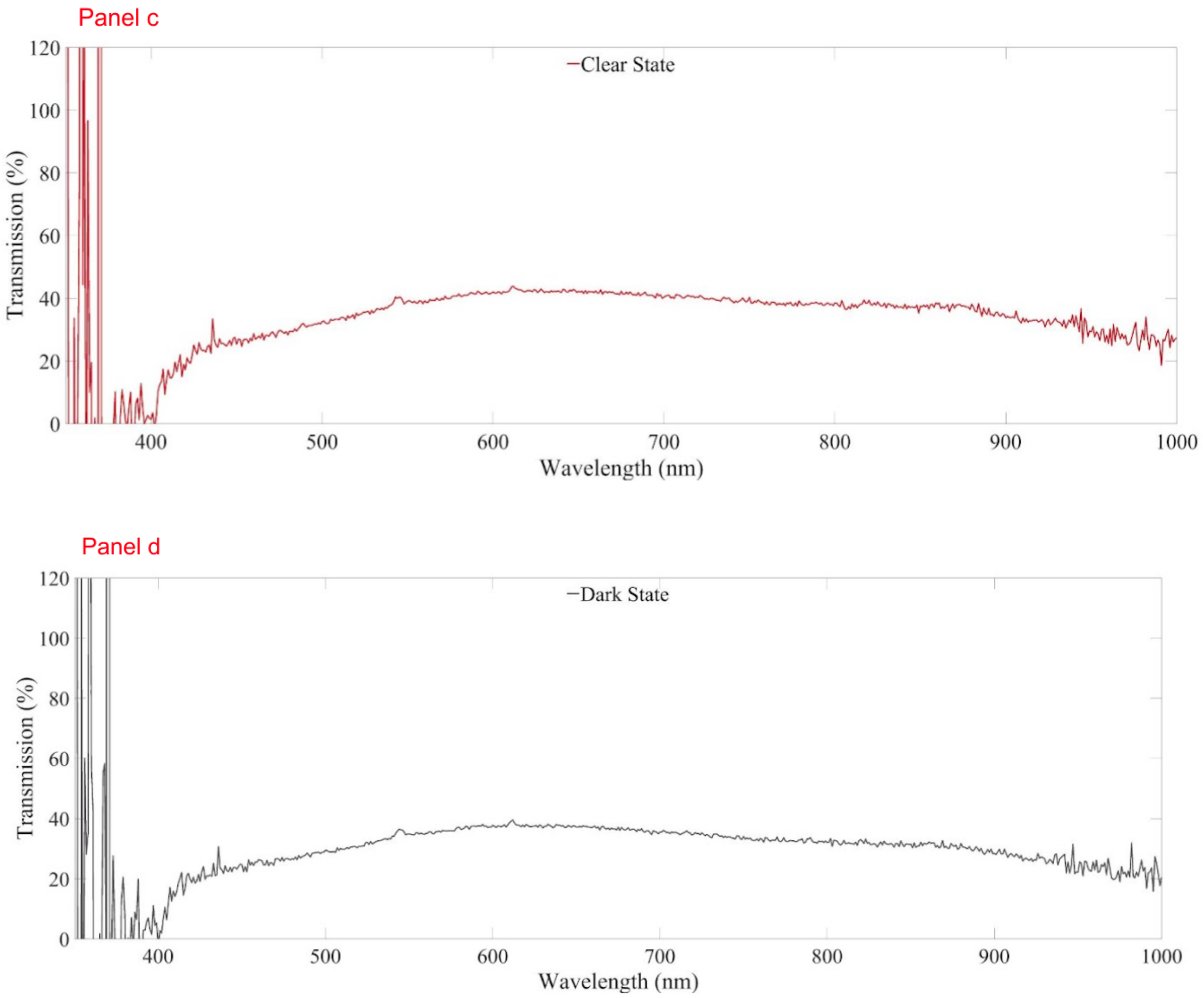

Figure 4: Results for the spectroscopic characterizations of the functional dynamic window in different states with different numbers of cycles. Panel a represents the spectroscopic characterization of window 1 clear state with 5.5 cycles. Panel b represents the spectroscopic characterization of window 1 dark state with 5.5 cycles. Panel c represents the spectroscopic characterization of window 1 clear state with 10 cycles. Panel d represents the spectroscopic characterization of window 1 dark state with 10 cycles.

To perform the strip-chart measurements, the 500 nm wavelength was selected for its ability to afford maximum uniform change of transmission between the dark and the transparent state of the window. The 500 nm wavelength also allowed us to avoid the noise fluctuation in the 420-500 nm.

Comparing panel c and panel d in Figure 5 as shown below and panel b in Figure 3 as shown before, we observed differences in the CV graphs despite the fabricated dynamic window using the same electrolyte as solution 5 from Lab 2. The possible reasons for the differences between the curve of solution 5 in Figure 3 panel b and Figure 5 panel c and panel d include the use of a two-electrode cell instead of a three-electrode cell in Lab 4, the lack of a true reference electrode in Lab 4, and the larger size of the working electrode in the dynamic window used in lab 4 than that used in Lab 2 which lead to a non-uniform deposition of metal on the FTO due to the voltage drop across the working electrode surface.

Panel a

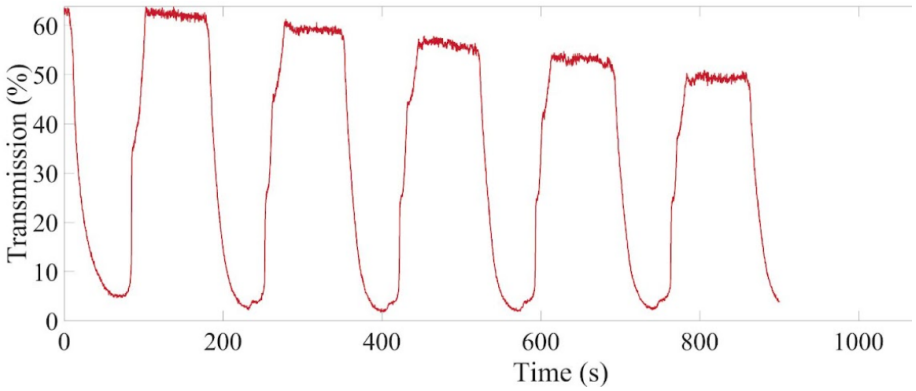

Panel b

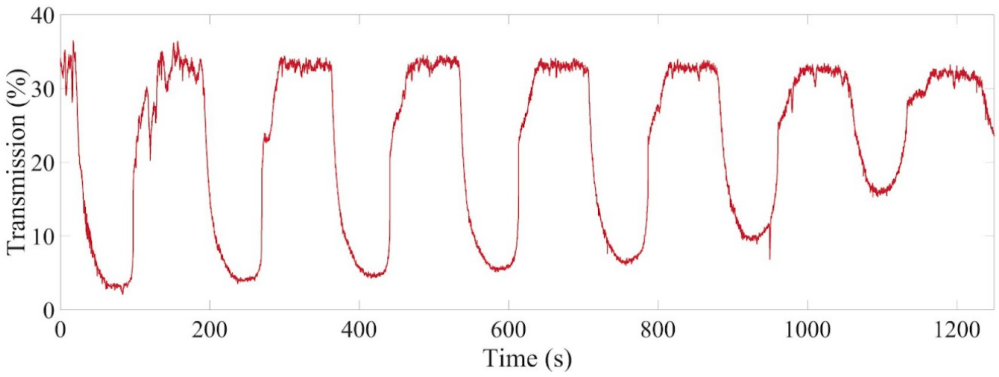

Panel c

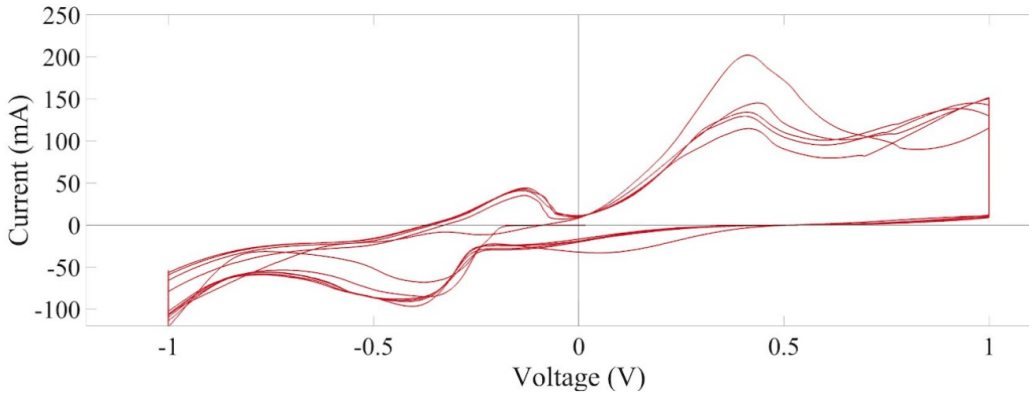

Panel d

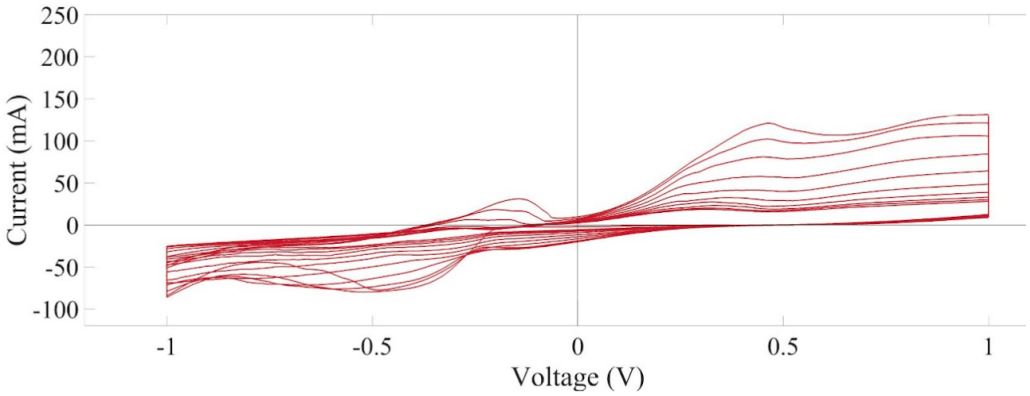

Panel e

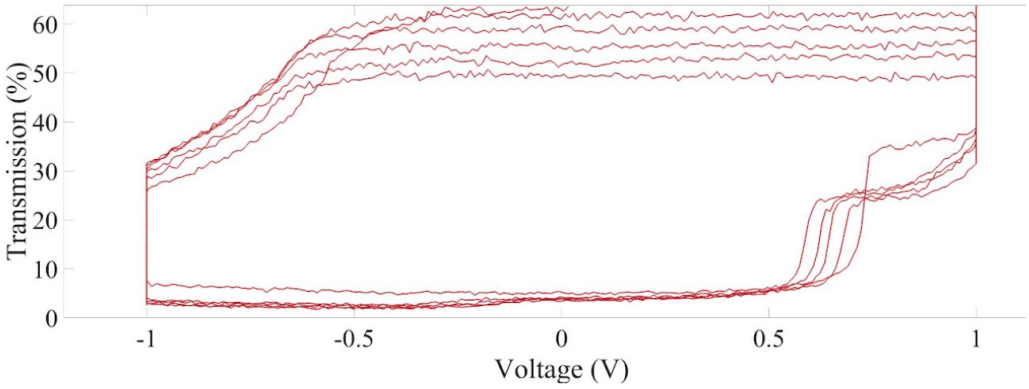

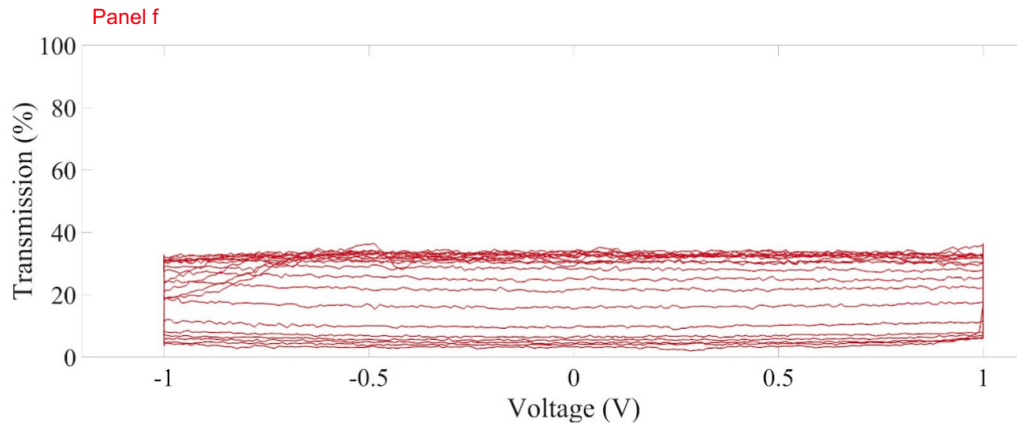

Figure 5: Results of the strip-chart measurements performed on the same dynamic window (window 1 as shown in Table 3) with different numbers of cycles. Panel a represents the transmission vs. time for window 1 with 5.5 cycles. Panel b represents transmission vs. time for window 1 with 10 cycles. Panel c represents the CV scan of window 1 with 5.5 cycles. Panel d represents the CV scan of window 1 with 10 cycles. Panel e represents transmission vs. voltage for window 1 with 5.5 cycles. Panel f represents the transmission vs. voltage for window 1 with 10 cycles.

Comparing panel a and panel b from Figure 5 as shown above, we saw that the maximum transmission value for each cycle of the dynamic window running with 5.5 cycles at its clear state decreased over time. On the other hand, the maximum transmission value for each cycle of the dynamic window running with 10 cycles at its clear state stayed relatively constant over time. However, we also observed that the minimum transmission value for each cycle of the dynamic window running with 5.5 cycles at its dark state stayed relatively constant over time, whereas the minimum transmission value for each cycle of the dynamic window running with 10 cycles at its dark state increased over time.

Comparing panel e and panel f from Figure 5 as shown above, we calculated the average maximum transmission rates and the average minimum transmission rates for the same dynamic window running with 5.5 cycles and 10 cycles. The average maximum transmission rate for the window running with 5.5 cycles was 55% and the average minimum transmission rate for the window running with 5.5 cycles was 5%. On the other hand, the average maximum transmission rate for the window running with 10 cycles was 30% and the average minimum transmission rate for the window running with 10 cycles was 10%. Therefore, we could see that window 1 with 5.5

cycles had a higher average maximum transmission rate and a lower average minimum transmission rate than window 1 with 10 cycles.

Lab 5

Maximum Window Estimation

Based on the data of the dry FTO we obtained from Lab 5 four-point probe measurements, we calculated the sheet resistance (R_s) of the FTO as $7.47 \pm 0.03\ \Omega$. Then we proceeded to use formula $L = \sqrt{\frac{2\Delta V}{JR_s}}$. L was the distance from the edge to the center of the dynamic window (in this case it was 5 cm). ΔV was the largest possible voltage drop from the edge to the center of the dynamic window based on the measurement in Lab 2 which was 0.6 V. J was the current density based on the measurement in Lab 2 which was $\frac{0.1\ A}{25\ cm^2} = 0.004\ A/cm^2$. By plugging all the values into the formula, we obtained the estimation of the maximum length of the window edge as $2L = 12.67\ cm$.

To increase the maximum window size, we can increase the largest possible voltage drop from the edge to the center of the dynamic window since this makes the deposition of metals easier and makes the reduction of H_2 harder. Moreover, we can also decrease the current density at the cost of having slower deposition and stripping processes. Finally, we can also reduce the sheet resistance by making the TCO of the dynamic window more conductive.

Unexpected Results and Disapproval of Hypothesis

The unexpected result we encountered in this study was that window 2 did not function properly. After discovering that we were not able to perform the strip-chart measurements on window 2, we measured the resistance of window 2 and observed that the resistance was as large as an open circuit which indicated that window 2 was not conductive. A possible reason for this was the improper connections among the different layers of window 2 during the fabrication process.

The strip-chart measurements of window 1 with different cycles showed that window 1 with 5.5 cycles had a different average maximum transmission rate in the clear state and a different average minimum transmission rate in the dark state than window 1 with 10 cycles.

Therefore, the results disproved our hypothesis that the dynamic windows we fabricated in this study were able to maintain constant transmission values at both the clear state and the dark state regardless of the number of cycling.

Conclusion

In this study, we found the functional dynamic window that we fabricated had an average maximum transmission rate of 55% when running with 5.5 cycles and an average minimum transmission rate of 5% when running with 5.5 cycles. On the other hand, the same window when running with 10 cycles had an average maximum transmission rate of 30% and an average minimum transmission rate of 10%.

Our hypothesis was not supported by the experimental results since the dynamic windows we fabricated in this study were not able to maintain constant transmission values at both the clear state and the dark state regardless of the number of cycling.